View metadata, citation and similar papers at core.ac.uk

brought to you by CORE

provided by Elsevier - Publisher Connector

Current Biology 24, 2366–2375, October 20, 2014 ©2014 Elsevier Ltd All rights reserved http://dx.doi.org/10.1016/j.cub.2014.08.039

Article

Doublecortin Recognizes the Longitudinal Curvature of the Microtubule End and Lattice

Susanne Bechstedt,[1] Kevan Lu,[1] and Gary J. Brouhard[1,*]
[1]Department of Biology, McGill University, 1205 Avenue Docteur Penfield, Montréal, QC H3A 1B1, Canada

Summary

Background: Microtubule ends have distinct biochemical and structural features from those of the lattice. Several proteins that control microtubule behavior can distinguish the end of a microtubule from the lattice. The end-binding protein EB1, for example, recognizes the nucleotide state of microtubule ends, which are enriched in GTP-tubulin. EB1 shares its binding site with Doublecortin (DCX), a protein expressed in developing neurons. We showed recently that DCX binds with highest affinity to microtubule ends.
Results: Here we show that DCX recognizes microtubule ends by a novel mechanism based on lattice curvature. Using single-molecule microscopy, we show that DCX "comets" do not elongate at faster microtubule growth rates and DCX does not recognize two out of three GTP analogs. We demonstrate that DCX binds with higher affinity to curved microtubule lattices than to straight ones. We find that curvature recognition is a property of single DCX molecules. Straightening of protofilaments (pfs) at microtubule ends with paclitaxel significantly attenuates end-recognition by DCX, but not EB1. Mutations in DCX found in patients with double cortex syndrome disrupted curvature recognition.
Conclusions: We propose a model in which DCX recognizes microtubule ends through specific interactions with their structure. We conclude that microtubule ends have two distinct features that proteins can recognize independently, namely a structural feature related to curvature and nucleotide state.

Introduction

Cells regulate the growth and shrinkage of microtubules primarily through action at microtubule ends. As such, microtubule ends are focal points of protein activity [1] where microtubule polymerases, depolymerases, and end-binding proteins participate in determining the fate of individual microtubules [2]. A basic question is how these proteins distinguish the end of a microtubule from the lattice.

Biochemically, tubulin is a GTPase and microtubule ends are stabilized by a "GTP cap" [3], an extended region in which tubulin dimers have enhanced, nucleotide-dependent lateral contacts [4]. Structurally, there is a lack of consensus, because the data describing microtubule ends are varied. In electron micrographs (EM) of growing microtubules, the ends are not always blunt. Rather, the ends are frequently tapered, with some protofilaments (pfs) extending beyond others and curving outward, both in vitro [5] and in mitotic PtK1 cells [6] and *S. pombe* [7]. Pfs may curve outward because of a kink observed at the intradimer interface of GTP-tubulin complexes [8, 9] as well as GMPCPP-tubulin [10], which is presumably straightened by incorporation into the lattice [11]. Pfs may also curve at the interdimer interface. Within a single microtubule, the curvature of pfs is variable [6]. Polymerizing microtubule ends in vitro have an average curvature of ~5° per dimer, while microtubule ends in mitotic Ptk1 cells are more curved (~15° per dimer) [6]. These outwardly curved pfs are often interpreted as "sheets" [12], a flattened array of pfs connected by lateral bonds that differ from the lateral bonds in the closed tube [10]. One possible explanation for the "sheet" phenomenon is a tapered microtubule end with two intrinsic curvatures: one that curves pfs outward and one that closes the pfs into a tube [13]. The balance of these competing curvatures produces a flattened "sheet." The variability in the EM data and in the conditions used to obtain them, however, has left the structure of microtubule ends open to debate.

The study of microtubule ends advanced significantly with the discovery of proteins that "track" them [14], especially the canonical end-binding protein EB1 [15]. Fluorescent end-binding proteins appear as "comets" at microtubule ends and are now widely used as markers for microtubule dynamics in live cells [16]. An early hypothesis was that end-binding proteins recognize the nucleotide state of tubulin, namely the GTP cap, although an alternative hypothesis relating to structural features was also put forward [14]. The mechanism was settled by experiments demonstrating that EB1 binds preferentially to microtubules built from GTP analogs, first GMPCPP [17] then GTPγS [18]. A cryo-EM reconstruction of EB1 bound to GTPγS microtubules showed that the calponin-homology domain of EB1 binds to microtubules at the vertex of four tubulin dimers and contacts helix H3 of β-tubulin, which coordinates GTP hydrolysis [4]. EB1 also contacts the region of α-tubulin that compacts upon GTP hydrolysis [19]. These results provide a plausible mechanism by which EB1 could recognize the GTP cap. Many other proteins autonomously recognize the microtubule end, including the microtubule depolymerase MCAK [20], the polymerase XMAP215 [21], the kinetochore complex Dam1 [22], and the neuronal microtubule-associated protein Doublecortin (DCX) [23]. It remains unclear, however, whether these proteins recognize the same feature of microtubule ends, namely their nucleotide state, as EB1 does.

EB1 shares its binding site with DCX [24], a microtubule-associated protein that is mutated in cases of subcortical band heterotopia and X-linked lissencephaly [25, 26]. The disease is caused by a breakdown in the radial migration of cortical neurons, a phenotype reproduced in an animal model based on in utero electroporation of RNAi constructs [27]. Work in cultured neurons indicates that DCX expression plays a role in collateral branching [28], arborization of dendrites, and axon elongation [29]. Consistent with these phenotypes, DCX appears to bind to microtubules in the leading processes of migrating neurons [30, 31], extending immature neurites, and growth cones [28]. DCX controls microtubule dynamics and stability in these regions, but the molecular mechanism(s) by which it does so remain unclear.

The contacts made by EB1 and DCX within their shared binding site are different: notably, the ubiquitin-like DC domains of

*Correspondence: gary.brouhard@mcgill.ca

CrossMark

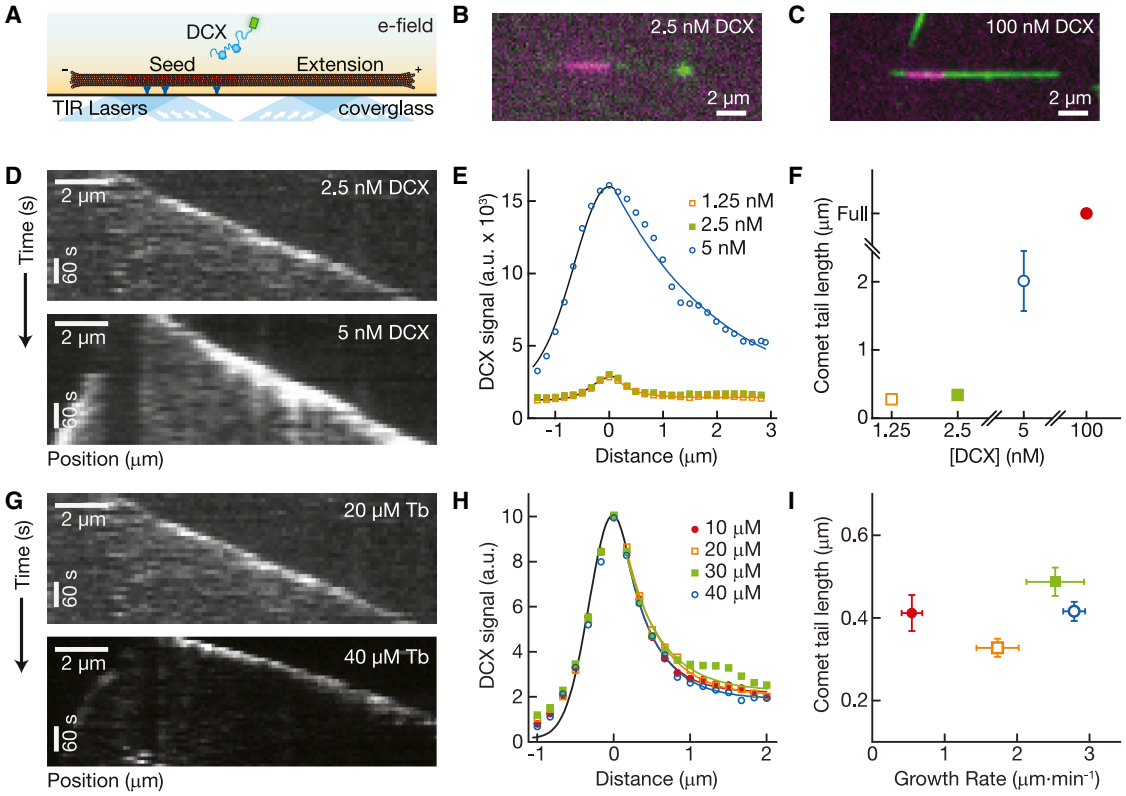

Figure 1. DCX Recognizes Microtubule Ends Differently Than EB1

(A) Schematic of the single molecule assay.
(B) Image of 2.5 nM DCX-GFP (green) binding to the end of a growing microtubule that extended from a seed (magenta).
(C) Image of 100 nM DCX-GFP (green) fully decorating the microtubule extension, creating the appearance of a "lightsaber."
(D) Kymographs depicting the interaction of 2.5 nM DCX-GFP (top) and 5 nM DCX-GFP (bottom) with dynamic microtubules. The signal is broader and more intense at 5 nM DCX-GFP than at 2.5 nM DCX-GFP.
(E) Plot of DCX-GFP intensity against the distance from the microtubule end at three different DCX-GFP concentrations (labeled).
(F) Plot of the comet length as a function of DCX-GFP concentration. The comet length increases with higher DCX-GFP concentration until the entire microtubule extension shows an equivalent DCX-GFP signal ("Full").
(G) Kymographs depicting the interaction of 2.5 nM DCX-GFP with dynamic microtubules at 20 μM tubulin (top) and 40 μM tubulin (bottom). The DCX-GFP signal is similar at the two tubulin concentrations.
(H) Plot of DCX-GFP intensity against the distance from the microtubule end at four different tubulin concentrations (labeled).
(I) Plot of the comet length as a function of tubulin concentration. The comet length does not vary systematically with tubulin concentration.
See also Figure S1.

DCX do not contact helix H3 of β-tubulin in the available EM reconstructions [4], although these reconstructions were performed with GDP microtubules only. In spite of this, we recently demonstrated that DCX binds with highest affinity to microtubule ends [23]. We were curious as to how DCX could recognize microtubule ends in the absence of the contacts found in EB1. We reasoned that DCX's end-tracking mechanism could provide an excellent model system for investigating the nature of microtubule ends. If DCX recognized a feature of microtubule ends distinct from nucleotide state, this result would inform the debate on their nature.

Using a single-molecule fluorescence microscopy assay [32], we sought to determine how DCX recognizes microtubule ends. We discovered four lines of evidence indicating that DCX and EB1 recognize distinct features at microtubule ends. DCX and EB1 differ in the way they "track" microtubule ends and in the way they bind to microtubules built with GTP analogs. Importantly, we discovered that DCX recognizes the longitudinal curvature of the microtubule lattice. Reducing the curvature of microtubule ends using paclitaxel attenuates end-recognition by DCX, but not EB1. Missense mutations found in patients disrupted the recognition of curved lattices and microtubule ends. Our results support a model in which DCX recognizes the microtubule end by a novel mechanism based on lattice curvature.

Results

DCX Comets Behave Differently Than EB1 Comets

We began our study with a comparison of end-tracking by DCX and EB1 using the single-molecule assay for microtubule-associated proteins [32]. Figure 1A shows a schematic of our experiment, in which single microtubule seeds are adhered to a cover glass surface. A dynamic microtubule extends from the seed. We added 2.5 nM recombinant DCX-GFP to our microscope chamber and observed preferential binding of DCX-GFP to growing microtubule ends. Figure 1B shows an image of this behavior (see Movie S1 available online), which is consistent with our previous observations [23]. This result indicates that the affinity of DCX-GFP is highest for the microtubule end. In other words, DCX recognizes a feature of the microtubule end that is distinct from the lattice.

Analysis of the size and shape of EB1-GFP comets has contributed several insights into the mechanism by which EB1 recognizes the GTP cap. First, the brightness of EB1-GFP decays exponentially along the length of the comet, which is consistent with the first-order temporal decay of EB1's binding site within the GTP cap [33]. Second, EB1-GFP comets elongate with increasing tubulin concentration, which is consistent with the GTP cap elongating at faster growth rates [33]. Third, increasing the EB1-GFP concentration causes the comets to shrink, suggesting that EB1 somehow catalyzes the destruction of its own binding site [18], perhaps by accelerating tubulin's GTPase activity through interactions with helix H3 of β-tubulin.

In order to determine whether DCX and EB1 recognize the same feature of microtubule ends, we asked whether DCX-GFP comets behave similarly. We first measured the size of DCX-GFP comets as we increased the DCX-GFP concentration in the reaction chamber at 10 μM tubulin. Figure 1D shows two kymographs of DCX-GFP tracking microtubule ends at 2.5 nM and 5 nM DCX-GFP (see Movie S2). The comets were brighter and longer at 5 nM DCX-GFP. We averaged the DCX-GFP signal of n > 50 comets and fit the result to an exponential decay function (Figure 1E, solid colored lines); the "comet length" is reported as the decay constant of the fit, λ [33]. Figure 1F shows a plot of comet length against DCX-GFP concentration. DCX comets elongated from λ = 0.41 ± 0.02 μm at 2.5 nM DCX-GFP, close to a diffraction-limited spot, until a point at which the entire extension grew outward with a bright DCX-GFP signal, as previously observed [23]. We refer to these fully decorated, bright extensions as "lightsabers" (Figure 1C). At no point did we observe a decreasing DCX-GFP signal at microtubule ends, which indicates that DCX does not catalyze the destruction of its own binding site. Whereas increasing the concentration of EB1 causes the comets to shrink, increasing the concentration of DCX causes the comets to grow.

We next asked whether DCX-GFP comets elongate with increasing tubulin concentration. We fixed the DCX-GFP concentration at 2.5 nM, varied the tubulin concentration, and measured the decay length of the DCX-GFP comets (Figure 1G). In agreement with published results, DCX-GFP did not itself change the microtubule growth rate ([34] see Figure S1), and the microtubules grew faster at higher tubulin concentrations, as expected. The comets remained close to a diffraction-limited spot in all cases (e.g., λ = 0.41 ± 0.02 μm at 10 μM tubulin and λ = 0.42 ± 0.02 μm at 40 μm tubulin, see Figure 1H). The plot in Figure 1I shows that comet length does not change systematically with increasing tubulin concentrations. In contrast, in our hands EB1-GFP comets elongated linearly with increasing tubulin concentrations (see Figure S1), growing from λ = 0.17 ± 0.04 μm at 10 μM tubulin to λ = 0.53 ± 0.05 μm at 60 μM tubulin, which is consistent with previous observations [33].

In order for a protein that recognizes microtubule ends to create a comet, the protein must dissociate rapidly after the microtubule end has "matured" into the final lattice. EB1, for example, has a dissociation rate constant of $k_d \approx 4\ s^{-1}$ at the microtubule end [33]. For DCX, the k_d depends on the DCX concentration due to the cooperative interactions that occur between DCX molecules. When many DCX molecules bind to adjacent sites on the microtubule lattice, their dissociation rate constants decrease significantly [23]. This fact enables us to interpret the transition of the DCX-GFP signal from comets to lightsabers. At 2.5 nM DCX-GFP, the signal is composed primarily of noninteracting single molecules of DCX-GFP, which have a dissociation rate constant of $k_d \approx 1.1\ s^{-1}$ [23]. This rapid dissociation of DCX creates the comets characteristic of end-tracking. As the DCX concentration increases, many DCX-GFP molecules will bind to the microtubule end within a short time window, and presumably the local concentration of DCX on the lattice becomes high enough for cooperative interactions between DCX molecules to occur. As a result, the DCX-GFP molecules dissociate more slowly and the comet elongates. At a sufficiently high concentration, the lattice will retain nearly all of its DCX-GFP molecules because of their very slow rate of dissociation. Nevertheless, DCX continues to recognize the microtubule end as its highest affinity substrate regardless of concentration, and thus the end continues to acquire a signal. The result is a lightsaber wherein DCX-GFP decorates the entire growing microtubule.

DCX Does Not Recognize Two out of Three GTP Analogs

The behavior of DCX-GFP comets suggested to us that DCX might recognize a distinct feature of microtubule ends. To test for a nucleotide mechanism, we asked whether DCX binds preferentially to microtubules built from GTP analogs. We adhered fluorescently labeled microtubules built with different GTP analogs to a cover glass surface. We measured the fluorescence intensity of DCX-GFP bound to microtubules built from GMPCPP, GTPγS, and GDP-BeF_3, and we compared this intensity with that measured on GDP microtubules in the same reaction chamber or in back-to-back experiments (see the Experimental Procedures). These experiments are complicated by the fact that DCX is highly cooperative, with a sigmoid binding curve that is optimized for 13 pf microtubules [23]. In fits of the DCX binding curves to the Hill equation, the *K* value and Hill coefficient are dominated by the pf-number of the underlying microtubules. GMPCPP microtubules have 14 pf [35], however, and the pf-numbers of GTPγS and GDP-BeF_3-microtubules are not well established. For this reason, the DCX-GFP concentration was set at 2.5 nM, a single-molecule concentration at which end-recognition is prominent and at which differences in binding based on pf-number are not detectable [23]. As a positive control, we performed the same analysis for 200 nM EB1-GFP, which binds preferentially to all three GTP analogs [17, 18]. As negative controls, we tested tau-GFP and kinesin-1-GFP, two MAPs that do not share the DCX/EB1 binding site [36–39] and have not been reported to interact differentially with microtubule ends.

Figure 2A shows the results for GMPCPP, namely box plots of the fluorescence intensity on GMPCPP microtubules divided by the intensity on GDP microtubules (see Figure S2 for raw intensity data). At 2.5 nM, DCX-GFP did not bind preferentially to GMPCPP microtubules ($I_{GMPCPP}/I_{GDP} = 0.97 \pm 0.16$). At 200 nM, EB1-GFP preferred GMPCPP microtubules ($I_{GMPCPP}/I_{GDP} = 1.36 \pm 0.12$), as expected [17], while tau and kinesin-1 did not. Historically, GMPCPP has been the primary GTP analog for microtubule research, in part because GMPCPP-tubulin polymerizes at the same rate as GTP-tubulin [40]. Recently, the analog GTPγS was shown to "mimic" the microtubule end for EB1, despite the fact that GTPγS-tubulin polymerizes very slowly and is not capable of spontaneous nucleation [18]. As shown in Figure 2B, we found that DCX-GFP bound preferentially to GTPγS microtubules ($I_{GTPγS}/I_{GDP} = 1.53 \pm 0.09$). EB1-GFP also preferred GTPγS microtubules ($I_{GTPγS}/I_{GDP} = 1.53 \pm 0.14$), as expected [18]. The binding of the negative control proteins, however, was also altered by GTPγS. At 10 nM, tau showed a clear preference for GTPγS microtubules ($I_{GTPγS}/I_{GDP} = 2.46 \pm 0.30$), as did 10 nM kinesin-1 ($I_{GTPγS}/I_{GDP} = 1.41 \pm 0.15$). Similar

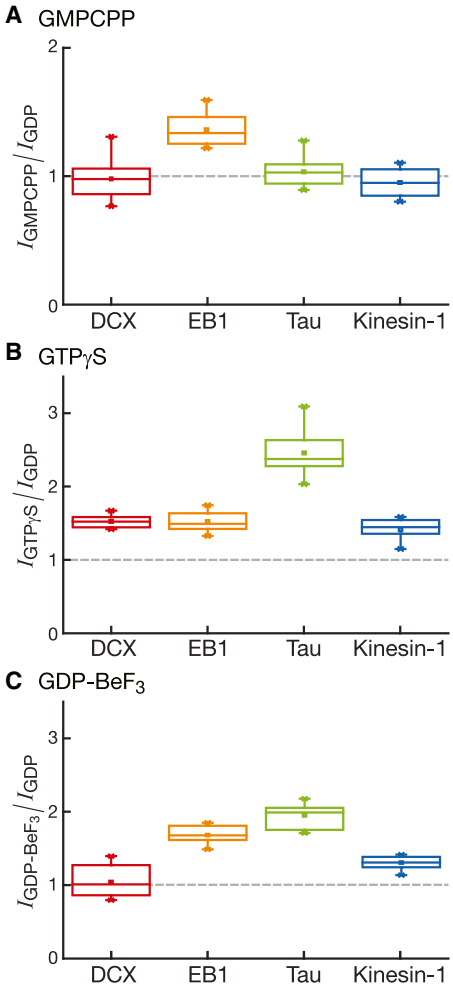

Figure 2. DCX Does Not Bind Preferentially to Microtubules Built from Two out of Three GTP Analogs

(A) Box plot of the intensity of fluorescent protein on a GMPCPP microtubule divided by the intensity on a GDP microtubule, I_{GMPCPP}/I_{GDP}. Data are shown for 2.5 nM DCX-GFP (red), 200 nM EB1-GFP (orange), 10 nM tau-GFP (green), and 10 nM kinesin-1-GFP (blue).

(B) Box plot of the intensity of fluorescent protein on a GTPγS microtubule divided by the intensity on a GDP microtubule, $I_{GTPγS}/I_{GDP}$. Data are shown for 2.5 nM DCX-GFP (red), 200 nM EB1-GFP (orange), 10 nM tau-GFP (green), and 10 nM kinesin-1-GFP (blue).

(C) Box plot of the intensity of fluorescent protein on a GDP-BeF_3 microtubule divided by the intensity on a GDP microtubule, $I_{GDP-BeF3}/I_{GDP}$. Data are shown for 2.5 nM DCX-GFP (red), 200 nM EB1-GFP (orange), 10 nM tau-GFP (green), and 10 nM kinesin-1-GFP (blue).

See also Figure S2.

pleiotropic effects were observed for GDP-BeF_3 (Figure 2C). DCX-GFP did not bind preferentially to GDP-BeF_3 microtubules ($I_{GDP-BeF3}/I_{GDP}$ = 1.03 ± 0.22), although EB1, tau, and kinesin-1 all preferred GDP-BeF_3. High-resolution structures of GTPγS and GDP-BeF_3 microtubules, similar to those of GMPCPP microtubules [19], will be necessary to determine the mechanism of these pleiotropic effects. While GTPγS microtubules were essential for the reconstruction of the EB1 binding site [4], our results indicate that GTPγS and GDP-BeF_3 can enhance the binding of MAPs that do not recognize microtubule ends and that have binding sites on the outer surface of the microtubule. For comparison, EB1 binds preferentially to all three GTP analogs, DCX binds preferentially only to GTPγS, and kinesin-1 and tau bind preferentially to GTPγS and GDP-BeF_3 analogs.

DCX Recognizes the Longitudinal Curvature of the Microtubule Lattice

Because DCX does not bind preferentially to two out of three GTP analogs we tested and DCX comets behave differently, we wondered if end-recognition might rely on structural features of microtubule ends. One hypothesis is that DCX might recognize the curvature of pfs frequently observed in EM. If this hypothesis is correct, we predict that DCX should recognize the longitudinal curvature of microtubules in other contexts. To test this prediction, we adhered microtubules to a cover glass surface in the presence of flow. Curved microtubules appear frequently in this process. We introduced 2.5 nM DCX-GFP into the flow chamber, a concentration at which end-recognition is apparent. Figure 3A shows an example image, and the curved microtubules showed a brighter DCX-GFP signal (see also Figure 3B and Movie S3). To confirm this observation, we measured the absolute curvature, $|\kappa|$, of our curved microtubules using a custom software application based on B-splines. Figure 3C shows a plot in which the DCX-GFP signal increases with the absolute curvature of the underlying microtubule lattice. The absolute curvature of our microtubules ranges from $|\kappa|$ = 0 to 2 μm^{-1}, corresponding to a maximum angular deflection of 1° per tubulin dimer (see the Supplemental Experimental Procedures). This angle is similar to that of polymerizing microtubule ends in vitro (5°) [6]. DCX-GFP may have higher affinity at curvatures greater than those accessible in our experiments. We repeated this experiment with 200 nM EB1-GFP (Figure 3D). No relationship between curvature and EB1-GFP brightness could be detected (Figure 3E), and the plot of EB1-GFP signal against $|\kappa|$ was flat (Figure 3F). These results indicate the DCX binds specifically to longitudinally curved microtubules.

How does DCX recognize a curved microtubule? Recognition of longitudinal curvature could be caused by cooperative interactions between DCX molecules, the means by which DCX recognizes lateral curvature and pf-number [23]. Alternatively, single DCX molecules might have higher affinity for curved microtubules. In order to distinguish between these possibilities, we introduced 0.25 nM DCX-GFP into a flow chamber containing curved microtubules (Figure 4A) and imaged the chamber continuously at 10 fps; single molecules were readily distinguished (Movie S4). We observed a higher frequency of single molecule events on curved regions (Figure 4B). To confirm that single molecules detected longitudinal curvature, we averaged the DCX-GFP signal over the experiment; the averaged signal is higher on curved regions (Figures 4C and 4D). To visualize this result another way, Figure 4E shows a kymograph of a curved microtubule; the measured curvature, $|\kappa|$, of the microtubule at each point is plotted above the kymograph. More events are observed in the curved region. These results indicate that the single molecule affinity of DCX-GFP for microtubules increases when the DCX binding site has been distorted by curvature and that DCX-GFP senses longitudinal curvature at the single molecule level while it senses lateral curvature by a cooperative mechanism. In a simplified view, there are four distortions possible in the DCX binding site of a curved microtubule: a convex bend, a concave bend, and the two transverse shear distortions on the top and bottom of the curved microtubule. One or more of these distortions must change the shape of the DCX binding site in a way that increases the DCX affinity for curved microtubules.

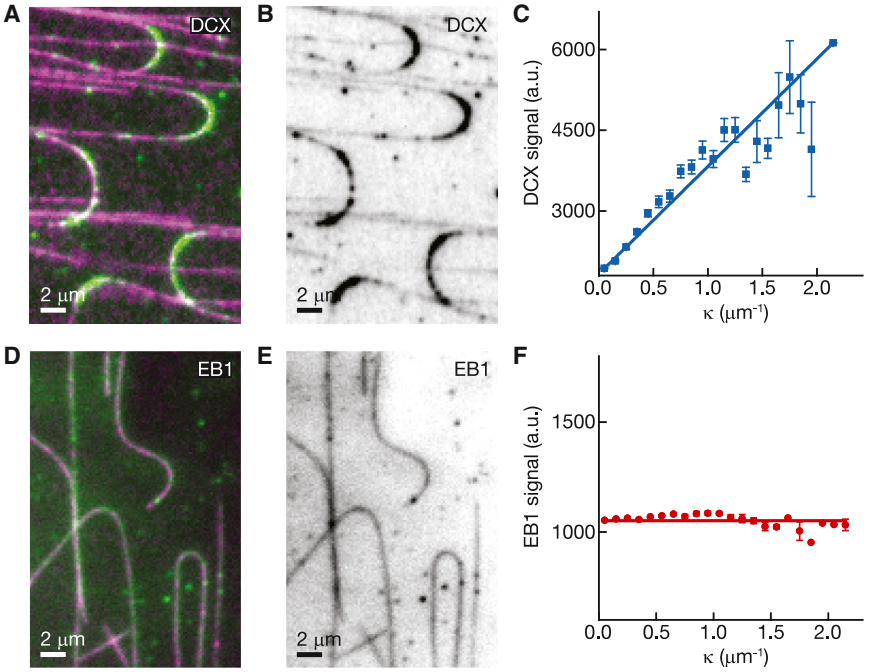

Figure 3. DCX Recognizes the Longitudinal Curvature of Microtubules

(A) Image of rhodamine-labeled microtubules (magenta) interacting with 2.5 nM DCX-GFP (green). A subset of the microtubules curve naturally while binding to the surface of the flow chamber. DCX-GFP is enriched on the curved segments.

(B) Inverted grayscale image of DCX-GFP taken from (A), showing the enrichment on curved microtubule segments.

(C) Plot of DCX-GFP intensity against the absolute curvature, $|\kappa|$, of the underlying microtubule. An approximately linear relationship between DCX-GFP signal and curvature is observed.

(D) Image of rhodamine-labeled microtubules (magenta) interacting with 200 nM EB1-GFP (green), including a subset of curved microtubules. EB1-GFP is not enriched on the curved segments.

(E) Inverted grayscale image of EB1-GFP taken from (D), showing the lack of enrichment on curved microtubule segments.

(F) Plot of EB1-GFP intensity against the absolute curvature, $|\kappa|$, of the underlying microtubule. No relationship between EB1-GFP signal and curvature is observed.

Straightening of Protofilaments Abolishes End-Recognition

If end-recognition by DCX relies on the curvature of protofilaments, the prediction is that straightening the pfs at microtubule ends should attenuate or abolish DCX end-recognition. We tested this prediction using paclitaxel, a microtubule-stabilizing chemotherapy drug, which has been shown to straighten pfs at microtubule ends [41, 42]. We added paclitaxel to our microtubule growth assays. Figures 5A and 5B show kymographs of DCX-GFP end-tracking with and without paclitaxel (note that the images were scaled independently). We observed a loss of the DCX-GFP end-tracking signal in the presence of paclitaxel (see Figure S3 for raw intensity data). We measured the ratio of the brightness at the end to the brightness on the lattice ($I_{End}/I_{Lattice}$, abbreviated here as I_E/I_L). For proteins that bind preferentially to microtubule ends, I_E/I_L is greater than 1. We measured I_E/I_L for DCX-GFP in both conditions, and paclitaxel significantly reduced the ratio (I_E/I_L = 6.65 ± 2.83 arbitrary units [a.u.] versus I_E/I_L = 2.13 ± 0.89 a.u., $p < 0.001$, see Figure 5C). In contrast, we did not observe changes in the I_E/I_L ratio for EB1-GFP with paclitaxel (Figures 5D–5F; I_E/I_L = 3.16 ± 1.47 a.u. versus I_E/I_L = 3.79 ± 1.24 a.u., $p = 0.33$). This result indicates that DCX end-recognition is sensitive to the curvature of pfs at microtubule ends.

Missense Mutations Found in Patients Disrupt Curvature Recognition

Our results above show that DCX recognizes the longitudinal curvature of microtubule ends and lattices. Is curvature recognition functionally significant? If so, we might expect that mutations that impair DCX function, namely those found in patients with double cortex syndrome, would be unable to recognize the longitudinal curvature in microtubules. Patient mutations in DCX cluster into tandem domains [43], the N-DC and C-DC domains, that have a common ubiquitin-like fold [44]. We previously tested eight N-DC mutations and seven C-DC mutations for their ability to bind cooperatively to microtubules and recognize their lateral curvature [23]. We expressed and purified these 15 mutants and tested them for recognition of longitudinal curvature at microtubule ends and lattices using the assays described above. We identified four mutations in the C-terminal DC domain for which longitudinal curvature recognition and end-tracking was abolished or severely reduced: R178L, P191R, T222I, and G223E. Figures 6A–6C show a homology model of the C-DC domain with the mutated residues highlighted. The four mutations map to three "corner sites" of the C-DC domain that are predicted to bind to tubulin residues at the vertex of four tubulin dimers [24]. Figure 6D shows an image of curved paclitaxel microtubules and one mutant, 25 nM R178L-DCX-GFP, interacting with these microtubules equally, regardless of curvature. Figure 6G shows a plot of GFP intensity against the $|\kappa|$ of the underlying microtubule for the four mutants, offset against each other for comparison. No correlation was measurable between $|\kappa|$ and intensity except for G223E, which showed residual curvature recognition. The same result was obtained at all concentrations tested. Similarly, Figure 6E shows a kymograph of another mutant, 25 nM P191R-DCX-GFP, interacting with a dynamic microtubule. No preferential binding to the end was observed. Figure 6H shows a box plot of I_E/I_L for wild-type DCX and the four mutants. The I_E/I_L ratio was reduced to ~1 for three of the mutants (e.g., I_E/I_L = 1.25 ± 0.29 for P191R-DCX-GFP). One mutant, G223E, showed less pronounced end-recognition (I_E/I_L = 7.36 ± 3.23 for DCX-GFP versus I_E/I_L = 4.48 ± 2.39 for G223E-DCX-GFP, $p < 0.05$). As above, the same results were obtained over a range of concentrations. Based on these findings, we designed two alanine substitutions (H205A and D213A) in the "fourth corner" of the C-DC domain [24], where no patient mutations have been reported. These two artificial mutants also displayed impaired curvature recognition and end-tracking (Figures 6G and 6H), which consolidates the conclusion that the C-DC domain is critical for recognition of longitudinal curvature. Despite their loss of curvature recognition, all of the mutants retained their preference for GTPγS microtubules (Figures 6F and 6I). Importantly, end-recognition and lattice-curvature recognition were both lost or reduced

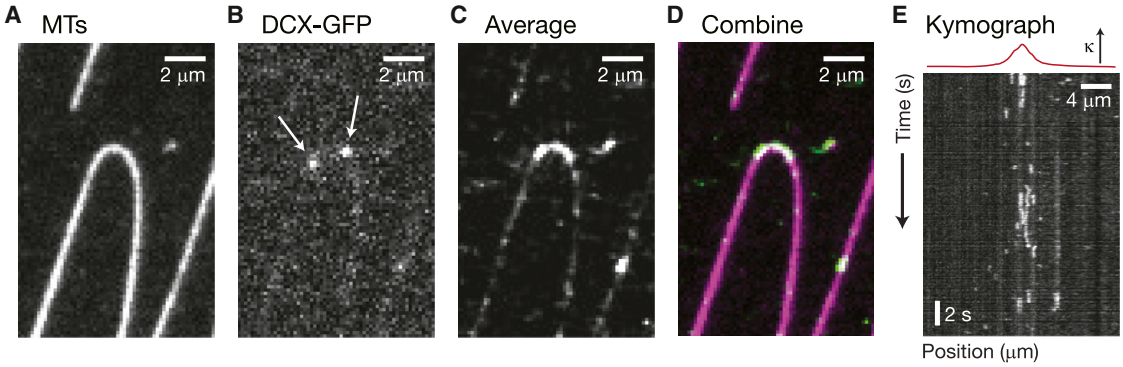

Figure 4. Single Molecules of DCX Recognize Longitudinal Curvature

(A) Image of curved paclitaxel microtubules.

(B) Image of 0.25 nM DCX-GFP interacting with the microtubules shown in (A). The white arrows point to single DCX-GFP molecules.

(C) Image of the average signal over 50 s of interactions between DCX-GFP and the microtubules shown in (A). A preference for the curved region of the microtubules is evident.

(D) Color-combined image of the DCX-GFP average (green) and the underlying microtubules (magenta).

(E) Kymograph showing DCX-GFP interacting with a curved microtubule. The red line above the kymograph shows the absolute curvature, $|\kappa|$, of the underlying microtubule. More events occur in the curved region of the microtubule.

in every case, indicating that these behaviors are linked. This linkage further supports the model that the recognition of microtubule ends occurs by recognition of a curved structure.

Discussion

Despite their common binding site at the vertex of four tubulin dimers, we now have four lines of evidence indicating that DCX and EB1 recognize distinct features at microtubule ends. First, DCX-GFP does not catalyze the destruction of its own binding site and DCX-GFP comets do not elongate at faster microtubule growth rates. Second, DCX-GFP does not bind preferentially to GMPCPP or GDP-BeF_3 microtubules. Third, DCX-GFP recognizes the longitudinal curvature of the microtubule lattice. Fourth, DCX-GFP end-recognition is attenuated by paclitaxel, which straightens pfs. DCX is a robust sensor of microtubule curvature, responding to minute changes in the microtubule lattice. These results lead us to propose that DCX recognizes microtubule ends by a novel mechanism based on lattice curvature.

We showed previously that DCX recognizes the lateral curvature of the microtubule lattice, a convex curve, by a mechanism that depends on cooperative interactions between neighboring DCX molecules [23]. Our results here have uncovered a novel behavior for DCX: its ability to recognize the longitudinal curvature of the microtubule lattice, a concave curve, at the single molecule level. To the best of our knowledge, DCX is the first microtubule-associated protein with this ability. Other microtubule-associated proteins respond differently to the "plasticity" and variable curvature of tubulin polymers. The microtubule polymerase Stu2p, for example, binds to a curved GTP-tubulin dimer [9]. Conversely, the kinetochore protein Ndc80 binds preferentially to intact microtubules over vinblastine-induced protofilament spirals [45], indicating a preference for straight lattices. Microtubule depolymerases of the kinesin-13 family may induce curvature in protofilaments as a way of promoting catastrophe and depolymerization [20]. In each case, curvature recognition is an integral part of current models for these proteins.

The loss of curvature recognition by four patient mutations in DCX suggests a functional role for this unique ability. DCX is active in regions in which microtubules can be highly curved [46], namely growth cones and the sites of collateral branch formation [28]. DCX may use curvature recognition in its interactions with microtubules in these regions. Indeed, a recent report indicated that RNAi of DCX caused aberrant microtubule curvature in growth cones [47], indicating that DCX may function to keep microtubule curvature within limits. Alternatively, DCX might recognize the longitudinal curvature of microtubule ends as a loading mechanism. Rather than binding directly to the microtubule lattice, where it might compete with other microtubule-associated proteins that sterically occlude its binding site, DCX could get a jump start on the lattice by loading onto the growing end. We previously argued that DCX recognizes microtubule ends because they are "polymerization intermediates," which would make them part of a mechanism to nucleate microtubules with exclusively 13 pfs [23]. If DCX plays a role in microtubule nucleation in the distal end of a neuronal process, then recognition of longitudinal curvature will allow it to target polymerization intermediates in the nucleation pathway. The patient mutants we tested may also suffer from localization defects, premature degradation, and/or aberrant posttranslational modifications that could also contribute to the disease phenotype. Nevertheless, the loss of curvature recognition by the four C-DC "corner mutants" is notable.

Our results support the notion that microtubule ends have two distinct features, namely a structural feature related to curvature and nucleotide state. This result implies that future models of microtubule growth must account for curvature at microtubule ends in addition to the recently established rapid kinetics of polymerization [48]. We remain agnostic about the atomic details of these curved features, given the variability in the EM data, where microtubule ends are alternately tapered and curved, sheet-like, or blunt. In schematics, microtubule ends are commonly drawn with a consistent, intrinsic outward curvature (e.g., [1]). Microtubule ends are presumably less stiff than closed tubes, however; a tapered end may sample a wider range of curvatures when distorted by thermal energy. Microtubule ends in cells are more curved than those found in solutions of pure tubulin [6], suggesting that proteins modulate the curvature of microtubule ends in vivo. We note that if all 13 pfs curved outward independently, cracks would appear

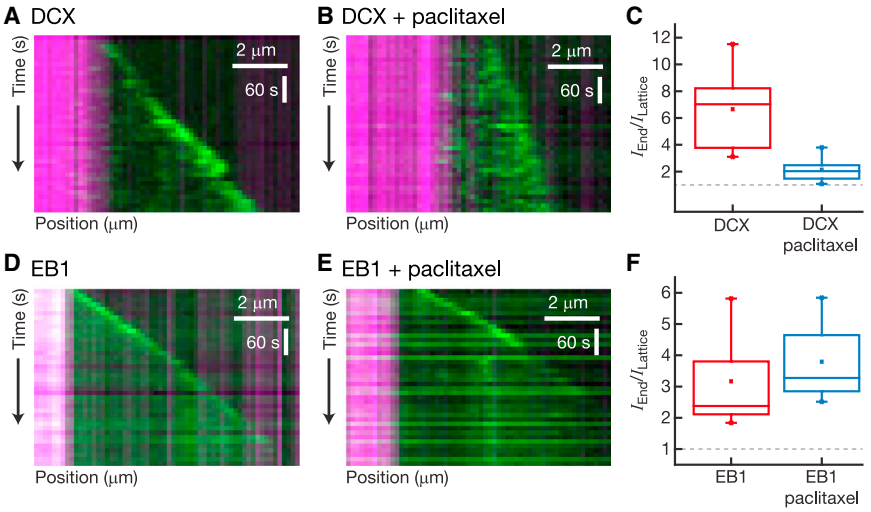

Figure 5. Straightening Protofilaments Attenuates DCX End-Tracking

(A) Kymograph showing the end-tracking behavior of 2.5 nM DCX-GFP at 10 μM tubulin.

(B) Kymograph showing the behavior of 2.5 nM DCX-GFP at 10 μM tubulin with 1 μM paclitaxel. The DCX-GFP signal at microtubule ends is not readily distinguishable from the lattice.

(C) Box plot of the intensities at microtubule ends divided by the intensities on the microtubule lattice for DCX-GFP in the presence and absence of paclitaxel. The $I_{End}/I_{Lattice}$ ratio is significantly reduced by the addition of paclitaxel.

(D) Kymograph showing the end-tracking behavior of 200 nM EB1-GFP at 10 μM tubulin.

(E) Kymograph showing the behavior of 200 nM EB1-GFP at 10 μM tubulin with 1 μM paclitaxel. The EB1-GFP signal at microtubule ends is not affected by the addition of paclitaxel.

(F) Box plot of the intensities at microtubule ends divided by the intensities on the microtubule lattice for EB1-GFP in the presence and absence of paclitaxel. The $I_{End}/I_{Lattice}$ ratio is not changed by the addition of paclitaxel.

See also Figure S3.

between adjacent pfs and destroy the DCX binding site. Therefore, curvature at microtubule ends must maintain lateral contacts between protofilaments, as occurs in models of sheet-like growth where the intrinsic outward curvature of pfs competes with the tendency of pfs to close into a tube [13].

There is more than one way to recognize a microtubule end. EB1 can recognize the nucleotide state but not curvature, while DCX recognizes curvature but does not recognize two out of three GTP analogs. Other proteins that recognize microtubule ends, such as XMAP215 and MCAK, might use still different mechanisms. At microtubule ends, changes in curvature might be linked to GTP hydrolysis events. The two features are separable, however, in that proteins can recognize one but not the other.

Experimental Procedures

Expression and Purification of DCX, EB1, tau, kinesin-1, and Mutant Constructs

The coding sequence for human Doublecortin (NCBI Reference Sequence Database accession number NP_835365) was a gift from Dr. Christopher Walsh. Human EB1 (GenBank accession number BC109281) was obtained from Thermo Scientific. The coding sequences for DCX and EB1 were PCR amplified using PfuX7 polymerase [49] and cloned into a pHAT protein expression vector as described [50]. The pHAT vector contained an N-terminal poly-His tag followed by a PreScission site and a C-terminal EGFP-tag followed by a *Strep*-tag II [51] for affinity purification. DCX-GFP was purified as described [23] (see the Supplemental Experimental Procedures for details). Missense mutations in DCX corresponding to those found in human patients were introduced using site-directed mutagenesis by the Kunkel method [52]. The cDNA for a constitutively active rat kinesin-1-GFP (rKin430-GFP) was a gift of Dr. Rob Cross to Dr. Jonathon Howard [53]. rKin430-GFP was expressed and purified as described [54]. The cDNA for human Tau (GenBank accession number BC114948) was obtained from Thermo Scientific and purified as described in the the Supplemental Experimental Procedures. Protein concentration and purity were determined using SDS-PAGE and absorbance at 280 nm and 488 nm using a NanoDrop spectrophotometer (Thermo Scientific). The eluted proteins were >99% pure in all cases. The proteins were used fresh and/or aliquots were flash frozen in LN_2 in the presence of 10% glycerol and stored in elution buffer.

Total Internal Reflection Fluorescence Microscopy and Preparation of Microscope Chambers

The single-molecule dynamic microtubule assay for microtubule-associated proteins was performed as described [32], with specific modifications described previously [23]. Microscope chambers were constructed using custom-machined mounts diagrammed in Gell et al. (2010). In brief, microscope cover glass were silanized as described [55]. A 22 × 22 mm glass and an 18 × 18 mm glass were separated by double-sided tape, such that a narrow channel was created for the exchange of solution. The standard imaging buffer is BRB80 + 10 μM paclitaxel + 0.1 mg/ml BSA + antifade reagents. Images were acquired using Metamorph. Simple measurements of microtubule intensities were made using the Linescan feature in Metamorph, and all intensity values are reported as mean ± SD. The absolute values of intensity are a function of laser power, laser alignment, and camera gain. Camera gain settings and laser powers were chosen to maximize the sensitivity and dynamic range of the camera, which prevents direct comparisons in intensity values between experiments in some cases. All experiments reported were repeated in a minimum of three independent trials.

Tubulin and Microtubule Preparations

Tubulin was purified from juvenile bovine brain homogenates as described [56]. Labeling of cycled tubulin with Alexa Fluor 546 or TAMRA (Invitrogen) was performed as described [57]; fluorescently labeled tubulin was typically used at a labeling ratio of 1:4 labeled:unlabeled tubulin dimers. Tubulin was polymerized into microtubules as follows.

Preparation of Paclitaxel-Stabilized GDP Microtubules

A polymerization mixture was prepared with BRB80 + 32 μM tubulin + 1 mM GTP + 4 mM $MgCl_2$ + 5% DMSO. The mixture was incubated on ice for 5 min, followed by incubation at 37°C for 30 min. The polymerized microtubules were diluted into prewarmed BRB80 + 10 μM paclitaxel, centrifuged at 110,000 rpm (199,000 × *g*) in a Beckman Airfuge, and resuspended in BRB80 + 10 μM paclitaxel.

Microtubule Polymerization in the Presence of GMPCPP

A polymerization mixture was prepared with BRB80 + 2 μM tubulin, 1 mM GMPCPP (Jena Biosciences), and 1 mM $MgCl_2$. The mixture was incubated on ice for 5 min, followed by incubation at 37°C for 2 hr. The polymerized GMPCPP microtubules were centrifuged at 110,000 rpm (199,000 × *g*) in a Beckman Airfuge and resuspended in BRB80.

Dynamic Microtubule Assay

Surface-immobilized GMPCPP microtubules were used to elongate dynamic microtubules in the presence of GTP. To grow dynamic microtubules from these "seeds," imaging buffer containing 10 μM tubulin, 1 mM GTP, and the protein concentration indicated in the text was introduced in the imaging chamber, which is heated to 35°C by an objective heater. For the DCX patient mutations, we tested a range of concentrations for each mutant (typically 2.5 nM to 100 nM) to account for the mutants' reduced cooperative binding to microtubules [23].

Comparison of GDP Microtubules and GMPCPP Microtubules

Microtubules were prepared as described in (1) and (2) above, with the modification that either the GDP microtubules or the GMPCPP microtubules were prepared with a lower ratio of fluorescently labeled tubulin, creating, for example, bright GMPCPP microtubules and dim GDP microtubules.

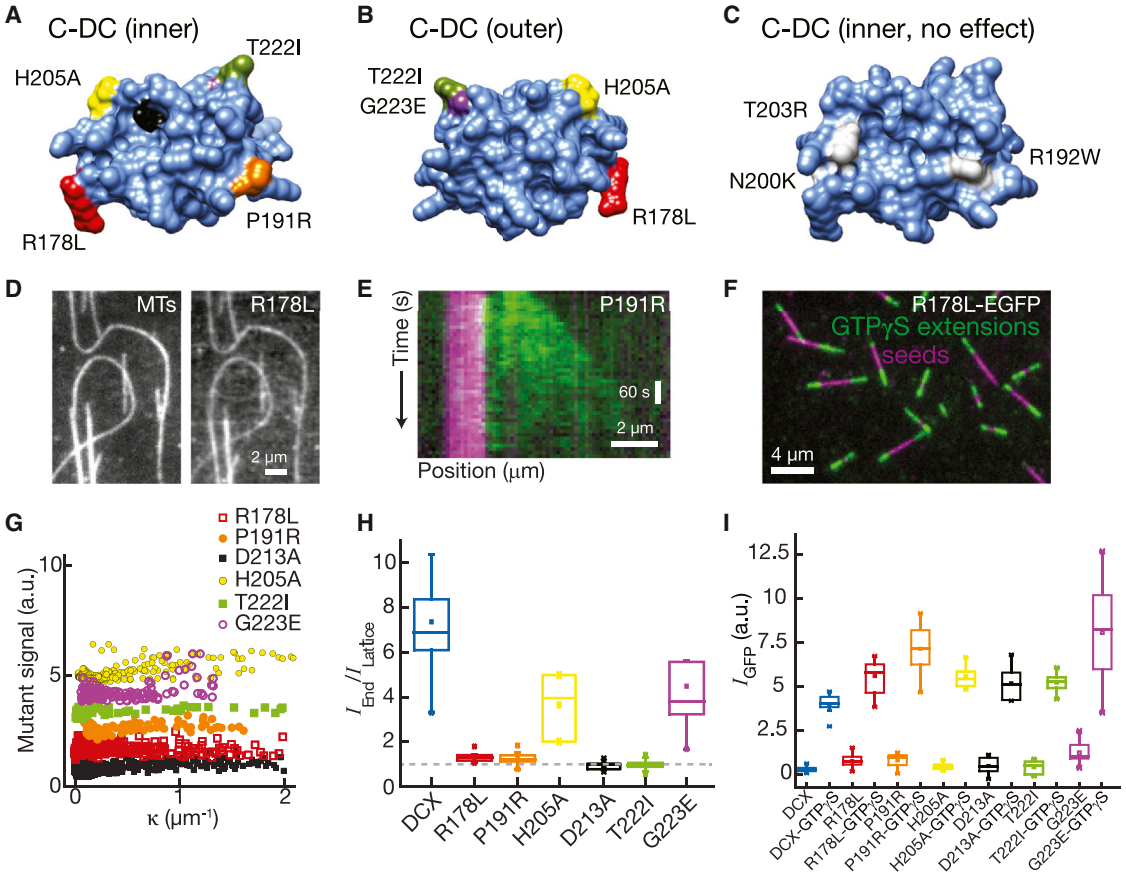

Figure 6. Missense Mutations in the C-DC Domain Disrupt Curvature Recognition

(A) Homology model of the C-DC domain based on an N-DC structure (Protein Data Bank accession number 2BQQ) from Fourniol et al. [24] showing the patient mutations used in this study.

(B) The homology model in (A) rotated 180°.

(C) Mutations in the C-DC domain that do not affect curvature recognition or end-tracking.

(D) Left: image of curved paclitaxel microtubules. Right: image of the signal averaged over 50 s of interaction between R178L-DCX-GFP and the microtubules shown at left.

(E) Kymograph depicting the interaction of 25 nM P191R-DCX-GFP with a dynamic microtubule. No preferential binding to microtubule ends is observed.

(F) Example image of a DCX mutant (R178L) binding preferentially to GTPγS extensions.

(G) Plot of GFP intensity against the absolute curvature, $|\kappa|$, of the underlying microtubule for the four C-DC mutants. No relationship between GFP signal and curvature is observed.

(H) Box plot of the ratio of intensities at microtubule ends divided by the intensities on the microtubule lattice for the four C-DC mutants tested at 20 nM, as well as for wild-type DCX at 2.5 nM. A ratio of 1 indicates an absence of preferential binding to microtubule ends.

(I) Box plot of intensities of DCX and mutations (20 nM) to GTPγS extensions and GMPCPP seeds.

See also Figure S4.

Both types of microtubules were adhered to the surface of the microscope chamber using anti-TAMRA antibodies as described [32].

Comparison of GDP Microtubules, GMPCPP Seeds, and GTPγS Extensions

GMPCPP microtubule seeds were adhered to a cover glass surface as described above. GTPγS-tubulin was used to elongate these seeds as described [18]. After elongation, paclitaxel-stabilized GDP microtubules were introduced into the flow chamber, where they settled onto the surface. The chamber was rinsed thoroughly and DCX-GFP or control proteins were introduced. In the case of EB1, the magnitude of its preference for GTP analogs is influenced by the presence of a His tag used for purification [18]. For this reason, we cloned, expressed, and purified a DCX-GFP construct that lacked a His tag in its sequence. The His-free DCX-GFP construct behaved identically to His-DCX-GFP-StrepII in all experiments presented here.

Comparison of GDP Microtubules, GMPCPP Seeds, and GDP-BeF_3 Extensions

GDP-BeF_3 extensions were prepared as GTPγS extensions with the exception that GTPγS was substituted with 1 mM GTP and 2 mM BeF_3 (Alfa Aesar). Because BeF_3 in solution can populate the nucleotide binding pocket of GDP microtubules, we compared GDP-BeF_3 extensions with GDP microtubules in back-to-back experiments.

Dynamic Assay in the Presence of Paclitaxel

Surface-immobilized GMPCPP-stabilized microtubules were used to elongate dynamic microtubules in the presence of GTP. To grow dynamic microtubules from these "seeds," imaging buffer containing 10 μM tubulin, 1 mM GTP, and 2.5 nM DCX-GFP or 200 nM EB1-GFP, with or without 1 μM paclitaxel, was introduced in the imaging chamber, which was heated to 35°C, and imaged.

Quantification of Curvature Recognition

Paclitaxel-stabilized GDP microtubules were introduced into a flow chamber as described above. Buffer flow was maintained during the time when microtubules settled onto the antibody-functionalized cover glass using filter paper. The continuous flow causes some microtubules to bend. DCX-GFP in imaging buffer was introduced to flow chambers containing curved microtubules and images were recorded. Quantification of the microtubule curvature, $|\kappa|$, and GFP signal on curved and straight microtubules was

analyzed using "Kappa," a custom software package based on cubic B-splines, which are splines comprised of piecewise degree-3 Bézier curves (K.L. and G.J.B., unpublished data; see the Supplemental Experimental Procedures for a complete description).

Supplemental Information

Supplemental Information includes Supplemental Experimental Procedures, four figures, and four movies and can be found with this article online at http://dx.doi.org/10.1016/j.cub.2014.08.039.

Acknowledgments

We thank Abattoir Jacques Forget (Terrebonne, Québec) for source material for tubulin purification. We thank S. Chaaban, J. Howard, J. Kollman, C. Moores, L. Rice, M. Wieczorek, and M. Zanic for comments on the manuscript. We thank S. Wolfson for editing. We thank G. Lucas for terminology. This work was supported by the Canadian Institutes of Health Research (CIHR, MOP-111265 to G.J.B.), by the Natural Sciences and Engineering Research Council of Canada (NSERC, #372593-09 to G.J.B.), and by McGill University. K.L. was supported by an NSERC Undergraduate Summer Research Award. G.J.B. is supported by a CIHR New Investigator Award.

Received: January 29, 2014
Revised: July 14, 2014
Accepted: August 15, 2014
Published: October 2, 2014

References

1. Akhmanova, A., and Steinmetz, M.O. (2008). Tracking the ends: a dynamic protein network controls the fate of microtubule tips. Nat. Rev. Mol. Cell Biol. *9*, 309–322.
2. Howard, J., and Hyman, A.A. (2007). Microtubule polymerases and depolymerases. Curr. Opin. Cell Biol. *19*, 31–35.
3. Mitchison, T., and Kirschner, M. (1984). Dynamic instability of microtubule growth. Nature *312*, 237–242.
4. Maurer, S.P., Fourniol, F.J., Bohner, G., Moores, C.A., and Surrey, T. (2012). EBs recognize a nucleotide-dependent structural cap at growing microtubule ends. Cell *149*, 371–382.
5. Mandelkow, E.M., Mandelkow, E., and Milligan, R.A. (1991). Microtubule dynamics and microtubule caps: a time-resolved cryo-electron microscopy study. J. Cell Biol. *114*, 977–991.
6. McIntosh, J.R., Grishchuk, E.L., Morphew, M.K., Efremov, A.K., Zhudenkov, K., Volkov, V.A., Cheeseman, I.M., Desai, A., Mastronarde, D.N., and Ataullakhanov, F.I. (2008). Fibrils connect microtubule tips with kinetochores: a mechanism to couple tubulin dynamics to chromosome motion. Cell *135*, 322–333.
7. Höög, J.L., Huisman, S.M., Sebö-Lemke, Z., Sandblad, L., McIntosh, J.R., Antony, C., and Brunner, D. (2011). Electron tomography reveals a flared morphology on growing microtubule ends. J. Cell Sci. *124*, 693–698.
8. Pecqueur, L., Duellberg, C., Dreier, B., Jiang, Q., Wang, C., Plückthun, A., Surrey, T., Gigant, B., and Knossow, M. (2012). A designed ankyrin repeat protein selected to bind to tubulin caps the microtubule plus end. Proc. Natl. Acad. Sci. USA *109*, 12011–12016.
9. Ayaz, P., Ye, X., Huddleston, P., Brautigam, C.A., and Rice, L.M. (2012). A TOG:αβ-tubulin complex structure reveals conformation-based mechanisms for a microtubule polymerase. Science *337*, 857–860.
10. Wang, H.W., and Nogales, E. (2005). Nucleotide-dependent bending flexibility of tubulin regulates microtubule assembly. Nature *435*, 911–915.
11. Rice, L.M., Montabana, E.A., and Agard, D.A. (2008). The lattice as allosteric effector: structural studies of alphabeta- and γ-tubulin clarify the role of GTP in microtubule assembly. Proc. Natl. Acad. Sci. USA *105*, 5378–5383.
12. Chrétien, D., Fuller, S.D., and Karsenti, E. (1995). Structure of growing microtubule ends: two-dimensional sheets close into tubes at variable rates. J. Cell Biol. *129*, 1311–1328.
13. Jánosi, I.M., Chrétien, D., and Flyvbjerg, H. (1998). Modeling elastic properties of microtubule tips and walls. Eur. Biophys. J. *27*, 501–513.
14. Perez, F., Diamantopoulos, G.S., Stalder, R., and Kreis, T.E. (1999). CLIP-170 highlights growing microtubule ends in vivo. Cell *96*, 517–527.
15. Morrison, E.E., Wardleworth, B.N., Askham, J.M., Markham, A.F., and Meredith, D.M. (1998). EB1, a protein which interacts with the APC tumour suppressor, is associated with the microtubule cytoskeleton throughout the cell cycle. Oncogene *17*, 3471–3477.
16. Matov, A., Applegate, K., Kumar, P., Thoma, C., Krek, W., Danuser, G., and Wittmann, T. (2010). Analysis of microtubule dynamic instability using a plus-end growth marker. Nat. Methods *7*, 761–768.
17. Zanic, M., Stear, J.H., Hyman, A.A., and Howard, J. (2009). EB1 recognizes the nucleotide state of tubulin in the microtubule lattice. PLoS ONE *4*, e7585.
18. Maurer, S.P., Bieling, P., Cope, J., Hoenger, A., and Surrey, T. (2011). GTPgammaS microtubules mimic the growing microtubule end structure recognized by end-binding proteins (EBs). Proc. Natl. Acad. Sci. USA *108*, 3988–3993.
19. Alushin, G.M., Lander, G.C., Kellogg, E.H., Zhang, R., Baker, D., and Nogales, E. (2014). High-resolution microtubule structures reveal the structural transitions in αβ-tubulin upon GTP hydrolysis. Cell *157*, 1117–1129.
20. Desai, A., Verma, S., Mitchison, T.J., and Walczak, C.E. (1999). Kin I kinesins are microtubule-destabilizing enzymes. Cell *96*, 69–78.
21. Brouhard, G.J., Stear, J.H., Noetzel, T.L., Al-Bassam, J., Kinoshita, K., Harrison, S.C., Howard, J., and Hyman, A.A. (2008). XMAP215 is a processive microtubule polymerase. Cell *132*, 79–88.
22. Lampert, F., Hornung, P., and Westermann, S. (2010). The Dam1 complex confers microtubule plus end-tracking activity to the Ndc80 kinetochore complex. J. Cell Biol. *189*, 641–649.
23. Bechstedt, S., and Brouhard, G.J. (2012). Doublecortin recognizes the 13-protofilament microtubule cooperatively and tracks microtubule ends. Dev. Cell *23*, 181–192.
24. Fourniol, F.J., Sindelar, C.V., Amigues, B., Clare, D.K., Thomas, G., Perderiset, M., Francis, F., Houdusse, A., and Moores, C.A. (2010). Template-free 13-protofilament microtubule-MAP assembly visualized at 8 A resolution. J. Cell Biol. *191*, 463–470.
25. Gleeson, J.G., Allen, K.M., Fox, J.W., Lamperti, E.D., Berkovic, S., Scheffer, I., Cooper, E.C., Dobyns, W.B., Minnerath, S.R., Ross, M.E., and Walsh, C.A. (1998). Doublecortin, a brain-specific gene mutated in human X-linked lissencephaly and double cortex syndrome, encodes a putative signaling protein. Cell *92*, 63–72.
26. des Portes, V., Pinard, J.M., Billuart, P., Vinet, M.C., Koulakoff, A., Carrié, A., Gelot, A., Dupuis, E., Motte, J., Berwald-Netter, Y., et al. (1998). A novel CNS gene required for neuronal migration and involved in X-linked subcortical laminar heterotopia and lissencephaly syndrome. Cell *92*, 51–61.
27. Bai, J., Ramos, R.L., Ackman, J.B., Thomas, A.M., Lee, R.V., and LoTurco, J.J. (2003). RNAi reveals doublecortin is required for radial migration in rat neocortex. Nat. Neurosci. *6*, 1277–1283.
28. Tint, I., Jean, D., Baas, P.W., and Black, M.M. (2009). Doublecortin associates with microtubules preferentially in regions of the axon displaying actin-rich protrusive structures. J. Neurosci. *29*, 10995–11010.
29. Deuel, T.A., Liu, J.S., Corbo, J.C., Yoo, S.Y., Rorke-Adams, L.B., and Walsh, C.A. (2006). Genetic interactions between doublecortin and doublecortin-like kinase in neuronal migration and axon outgrowth. Neuron *49*, 41–53.
30. Gleeson, J.G., Lin, P.T., Flanagan, L.A., and Walsh, C.A. (1999). Doublecortin is a microtubule-associated protein and is expressed widely by migrating neurons. Neuron *23*, 257–271.
31. Francis, F., Koulakoff, A., Boucher, D., Chafey, P., Schaar, B., Vinet, M.C., Friocourt, G., McDonnell, N., Reiner, O., Kahn, A., et al. (1999). Doublecortin is a developmentally regulated, microtubule-associated protein expressed in migrating and differentiating neurons. Neuron *23*, 247–256.
32. Gell, C., Bormuth, V., Brouhard, G.J., Cohen, D.N., Diez, S., Friel, C.T., Helenius, J., Nitzsche, B., Petzold, H., Ribbe, J., et al. (2010). Microtubule dynamics reconstituted in vitro and imaged by single-molecule fluorescence microscopy. Methods Cell Biol. *95*, 221–245.
33. Bieling, P., Laan, L., Schek, H., Munteanu, E.L., Sandblad, L., Dogterom, M., Brunner, D., and Surrey, T. (2007). Reconstitution of a microtubule plus-end tracking system in vitro. Nature *450*, 1100–1105.
34. Moores, C.A., Perderiset, M., Kappeler, C., Kain, S., Drummond, D., Perkins, S.J., Chelly, J., Cross, R., Houdusse, A., and Francis, F. (2006). Distinct roles of doublecortin modulating the microtubule cytoskeleton. EMBO J. *25*, 4448–4457.
35. Meurer-Grob, P., Kasparian, J., and Wade, R.H. (2001). Microtubule structure at improved resolution. Biochemistry *40*, 8000–8008.

36. Al-Bassam, J., Ozer, R.S., Safer, D., Halpain, S., and Milligan, R.A. (2002). MAP2 and tau bind longitudinally along the outer ridges of microtubule protofilaments. J. Cell Biol. *157*, 1187–1196.
37. Hirose, K., Lockhart, A., Cross, R.A., and Amos, L.A. (1995). Nucleotide-dependent angular change in kinesin motor domain bound to tubulin. Nature *376*, 277–279.
38. Hoenger, A., Sablin, E.P., Vale, R.D., Fletterick, R.J., and Milligan, R.A. (1995). Three-dimensional structure of a tubulin-motor-protein complex. Nature *376*, 271–274.
39. Kikkawa, M., Ishikawa, T., Wakabayashi, T., and Hirokawa, N. (1995). Three-dimensional structure of the kinesin head-microtubule complex. Nature *376*, 274–277.
40. Hyman, A.A., Salser, S., Drechsel, D.N., Unwin, N., and Mitchison, T.J. (1992). Role of GTP hydrolysis in microtubule dynamics: information from a slowly hydrolyzable analogue, GMPCPP. Mol. Biol. Cell *3*, 1155–1167.
41. Elie-Caille, C., Severin, F., Helenius, J., Howard, J., Muller, D.J., and Hyman, A.A. (2007). Straight GDP-tubulin protofilaments form in the presence of taxol. Curr. Biol. *17*, 1765–1770.
42. Zanic, M., Widlund, P.O., Hyman, A.A., and Howard, J. (2013). Synergy between XMAP215 and EB1 increases microtubule growth rates to physiological levels. Nat. Cell Biol. *15*, 688–693.
43. Taylor, K.R., Holzer, A.K., Bazan, J.F., Walsh, C.A., and Gleeson, J.G. (2000). Patient mutations in doublecortin define a repeated tubulin-binding domain. J. Biol. Chem. *275*, 34442–34450.
44. Kim, M.H., Cierpicki, T., Derewenda, U., Krowarsch, D., Feng, Y., Devedjiev, Y., Dauter, Z., Walsh, C.A., Otlewski, J., Bushweller, J.H., and Derewenda, Z.S. (2003). The DCX-domain tandems of doublecortin and doublecortin-like kinase. Nat. Struct. Biol. *10*, 324–333.
45. Alushin, G.M., Ramey, V.H., Pasqualato, S., Ball, D.A., Grigorieff, N., Musacchio, A., and Nogales, E. (2010). The Ndc80 kinetochore complex forms oligomeric arrays along microtubules. Nature *467*, 805–810.
46. Dent, E.W., Callaway, J.L., Szebenyi, G., Baas, P.W., and Kalil, K. (1999). Reorganization and movement of microtubules in axonal growth cones and developing interstitial branches. J. Neurosci. *19*, 8894–8908.
47. Jean, D.C., Baas, P.W., and Black, M.M. (2012). A novel role for doublecortin and doublecortin-like kinase in regulating growth cone microtubules. Hum. Mol. Genet. *21*, 5511–5527.
48. Gardner, M.K., Charlebois, B.D., Jánosi, I.M., Howard, J., Hunt, A.J., and Odde, D.J. (2011). Rapid microtubule self-assembly kinetics. Cell *146*, 582–592.
49. Nørholm, M.H. (2010). A mutant Pfu DNA polymerase designed for advanced uracil-excision DNA engineering. BMC Biotechnol. *10*, 21.
50. Bitinaite, J., Rubino, M., Varma, K.H., Schildkraut, I., Vaisvila, R., and Vaiskunaite, R. (2007). USER friendly DNA engineering and cloning method by uracil excision. Nucleic Acids Res. *35*, 1992–2002.
51. Schmidt, T.G., and Skerra, A. (2007). The Strep-tag system for one-step purification and high-affinity detection or capturing of proteins. Nat. Protoc. *2*, 1528–1535.
52. Kunkel, T.A. (1985). Rapid and efficient site-specific mutagenesis without phenotypic selection. Proc. Natl. Acad. Sci. USA *82*, 488–492.
53. Rogers, K.R., Weiss, S., Crevel, I., Brophy, P.J., Geeves, M., and Cross, R. (2001). KIF1D is a fast non-processive kinesin that demonstrates novel K-loop-dependent mechanochemistry. EMBO J. *20*, 5101–5113.
54. Varga, V., Leduc, C., Bormuth, V., Diez, S., and Howard, J. (2009). Kinesin-8 motors act cooperatively to mediate length-dependent microtubule depolymerization. Cell *138*, 1174–1183.
55. Helenius, J., Brouhard, G., Kalaidzidis, Y., Diez, S., and Howard, J. (2006). The depolymerizing kinesin MCAK uses lattice diffusion to rapidly target microtubule ends. Nature *441*, 115–119.
56. Castoldi, M., and Popov, A.V. (2003). Purification of brain tubulin through two cycles of polymerization-depolymerization in a high-molarity buffer. Protein Expr. Purif. *32*, 83–88.
57. Hyman, A., Drechsel, D., Kellogg, D., Salser, S., Sawin, K., Steffen, P., Wordeman, L., and Mitchison, T. (1991). Preparation of modified tubulins. Methods Enzymol. *196*, 478–485.